Journal of Knot Theory and Its Ramifications
© World Scientific Publishing Company

GENERALISED ATMOSPHERIC SAMPLING OF KNOTTED POLYGONS

E.J. JANSE VAN RENSBURG[1] AND A. RECHNITZER[2]

[1]*Department of Mathematics and Statistics, York University, Toronto, ON, Canada M3J 1P3*
[2]*Department of Mathematics, University of British Columbia, Vancouver, BC, Canada V6T 1Z2*

ABSTRACT

Self-avoiding polygons in the cubic lattice are models of ring polymers in dilute solution. The conformational entropy of a ring polymer is a dominant factor in its physical and chemical properties, and this is modeled by the large number of conformations of lattice polygons. Since cubic lattice polygons are embeddings of the circle in three space, they can be knotted is a model of knotting in ring polymers. In this paper we study the effects of knotting on the conformational entropy of lattice polygons and so determine the relative fraction of polygons of different knot types at large lengths.

More precisely, we consider the number of cubic lattice polygons of n edges and knot type K, $p_n(K)$. Numerical evidence strongly suggests that

$$p_n(K) \simeq C_K \; n^{\alpha-3+N_K} \; \mu_0^n$$

as $n \to \infty$, where μ_0 is the growth constant of unknotted lattice polygons, α is the entropic exponent of lattice polygons, and N_K is the number of prime knot components in the knot type K [35]. Determining the exact value of $p_n(K)$ is far beyond current techniques for all but very small values of n. Instead we use the GAS algorithm [23] to enumerate $p_n(K)$ approximately. We then extrapolate ratios $[p_n(K)/p_n(L)]$ to larger values of n for a number of given knot types.

We give evidence that for the unknot 0_1 and the trefoil knot 3_1, there exists a number $M_{0_1,3_1} \approx 170000$ such that $p_n(0_1) > p_n(3_1)$ if $n < M_{0_1,3_1}$ and $p_n(0_1) \leq p_n(3_1)$ if $n \geq M_{0_1,3_1}$. In addition, the asymptotic relative frequencies for a variety of knot types are determined. For example, we find that $[p_n(3_1)/p_n(4_1)] \to 27.0 \pm 2.2$, so that there are approximately 27 polygons of knot type the trefoil for every polygon of knot of type 4_1 (the figure eight knot), in the asymptotic limit.

Finally, we examine the dominant knot types at moderate values of n and conjecture that the most frequent knot types in polygons of any given length n, are of the form $K_+(N) = (3_1^+)^{\lceil N/2 \rceil} \# (3_1^-)^{\lfloor N/2 \rfloor}$ (or its chiral partner), where $3_1^+, 3_1^-$ are right- and left-handed trefoils, and N increases with n.

Keywords: Knotted Polygons, Monte Carlo, Lattice Knot Statistics.

AMS Mathematics Subject Classification 2000: 57M25, 82B41, 26D15, 92B99; PACS Numbers: 02.10.Kn, 36.20.Ey, 05.70.Jk, 87.15.Aa

1. Introduction

The statistics of ring polymers in dilute solution can be modeled by lattice polygons with excluded volume in three dimensions [5]. The most basic question in this model

is the determination of p_n, the number of self-avoiding polygons in $\mathbb{Z}^3$, a difficult and unsolved combinatorial problem in statistical mechanics [13]. This model is closely related to the self-avoiding walk model of excluded volume in linear polymers [14,12,8,9,5,30].

A lattice polygon is an unrooted embedding of the unlabeled cycle graph in the hypercubic lattice $\mathbb{Z}^d$. The length of the polygon is the number of unit length edges it contains and p_n is defined as the number of polygons of length n counted up to equivalence under translation in the lattice. The limit

$$\mu = \lim_{n\to\infty} p_n^{1/n} \tag{1.1}$$

is known to exist and μ is the lattice dependent growth constant and it is equal to that of self-avoiding walks [13]. Thus p_n grows exponentially, $p_n = \mu^{n+o(n)}$ and it is generally believed that its asymptotic growth is given by

$$p_n = An^{\alpha-3}\mu^n(1+o(1)) \tag{1.2}$$

where α is the *polygon entropic exponent* (or *specific heat exponent*). The function p_n also satisfies the limiting relation

$$\lim_{n\to\infty} \frac{p_{n+2}}{p_n} = \mu^2, \tag{1.3}$$

a result due to Kesten [27,28]; a simpler proof of this can be found in reference [30].

In the square lattice $\mathbb{Z}^2$ the numerical value of μ has been estimated using a variety of different methods, including computer enumeration and series analysis of square lattice polygons [25,26]. The best estimates for μ and α is:

$$\mu = 2.63815853034(10), \tag{1.4}$$

$$\alpha = 0.5000005(10) \tag{1.5}$$

A slight improvement can be found in reference [25][a]. The exponent α has also been estimated using conformal field theory and Coulomb gas methods, giving the exact value $\alpha = 1/2$ in two dimensions [33,34].

Estimates of μ and α in $\mathbb{Z}^3$ are less accurate (mostly due to the difficulty of computing p_n for even modest values of n). A good estimate for μ was obtained in reference [4]:

$$\mu = 4.684044(11), \tag{1.6}$$

$$\alpha \approx 0.24 \tag{1.7}$$

This estimate is based on the analysis of exact enumeration data generated by the lace expansion. The exponent α in three dimensions has also been determined by ϵ-expansion techniques [11,29], giving $\alpha = 0.237 \pm 0.002$.

The main focus of this paper is the number of polygons of length n and knot type K, $p_n(K)$, as measure of the conformational entropy of this class of polygons.

[a]Error bars and confidence intervals are those claimed in the original references.

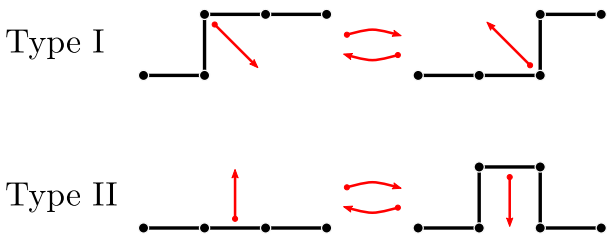

Fig. 1. The two elementary moves in the BFACF algorithm. Moves of type I are length preserving, while moves of type II changes the length of the polygon by two steps or edges.

These polygons are constrained by both self-avoidance and the topology of the embedding. It is widely believed that $p_n(K) \sim C_K n^{\alpha_K - 3} \mu_0^n$, where $\mu_0 < \mu$ [36,44], and there are evidence that the entropic exponent of unknots, α_{0_1} is equal to α, the entropic exponent of three dimensional polygons [35].

Unfortunately, computing $p_n(K)$ remains an exponential time problem and so we turn to approximate enumeration techniques. In reference [39] a new statistic called the *atmosphere* of a self-avoiding walk was introduced. This statistic was shown (numerically) to converge to the growth constant μ as the length of the walk increases. This subsequently [40] led to GARM, a generalisation of the Rosenbluth algorithm [14,41]. Like Rosenbluth sampling, GARM can be considered an approximate enumeration algorithm which forms precise estimates of the number of conformations of a given size. It may be enhanced by pruning and enrichment in a similar manner to Grassberger's PERM algorithm [10], and flat histogram techniques such as in [3,37]. The algorithm proved effective in sampling self-avoiding walks, but cannot sample polygons in the cubic lattice. This deficiency was overcome in [23] and the resulting GAS algorithm (Generalised Atmospheric Sampling) can be used to approximate the number of polygons of fixed knot type.

In this paper we use GAS to sample polygons of fixed knot types using BFACF-moves [2,1] as our basic "atmospheric moves" in the algorithm. These moves are known to have ergodicity classes which coincide with the knot types of polygons in the cubic lattice [16]. Running the algorithm on different knot types gives us estimates of $p_n(K)$ which we then compare and contrast. This allows us, for example, to determine the relative frequencies of different knot types.

In Section 2 we give a brief overview of the implementation of the GAS algorithm to sample polygons of fixed knot types. Some preliminary results of our simulations are given in Section 3. We discuss in particular the sieving of polygons of fixed knot types and minimal length - this is essential to the approximate enumeration of $p_n(K)$. Our data complement results obtained in reference [42], in which the BFACF algorithm was used to count (exactly) the numbers of polygons of minimal length and given knot type.

In Section 4 we present our numerical results for a range of knots types. We give

results on minimal knots in the cubic lattice; we state lower bounds on the number of distinct shortest polygons of a given knot type. We describe the approximate determination of $p_n(K) \simeq C_K n^{\alpha_k - 3} \mu_K^n$ for various knot types and discuss the calculation of amplitude ratios C_K/C_L of knot types K and L. We show how these results can be used to relate $p_n(K)$ and $p_n(L)$.

In Section 4.2 we discuss the unknot and the trefoil in some detail. We determine the amplitude ratio and show (numerically) that there is a number $M_{0_1,3_1}$ such that $p_n(0_1) \geq p_n(3_1)$ for $n \leq M_{0_1,3_1}$ and $p_n(0_1) < p_n(3_1)$ for $n > M_{0_1,3_1}$. In this case, our numerical data show that $M_{0_1,3_1} \approx 170000$. In Sections 4.3 and 4.4 we present data for the figure eight knot 4_1 as well as $5_1, 6_1, 6_2, 6_3$ and 8_{19}. Our data show, in particular, that $p_n(3_1)/p_n(4_1) \to 27.0 \pm 2.2$ as $n \to \infty$, implying that for large values of n the trefoil knot type is about 27 times more abundant than the figure eight knot type. Similar results are presented for other knot types.

In Section 5 we present results for some compound knots. We consider the relative frequencies of knots of types $3_1\#3_1$, $3_1\#4_1$ and $4_1\#4_1$, and also knots with three prime components of type trefoil. These results lead us to conjecture that the most abundant knot type in cubic lattice polygons is $K_+(N) = (3_1^+)^{\lceil N/2 \rceil} \# (3_1^-)^{\lfloor N/2 \rfloor}$ (or its chiral partner $K_-(N)$), where 3_1^+ and 3_1^- are right and left handed trefoils and N is an increasing function of the polygon length n.

We conclude the paper in Section 6 with a few final observations and comments.

2. The Entropy of Knotted Polygons

Let K be a given knot type and consider the number $p_n(K)$ of polygons of knot type K and length n. Before we begin the main body of this section, a few remarks on chirality are in order.

If K is a chiral knot type, then we denote its right- and left-handed types by K^+ and K^-. Observe that

$$p_n(K^+) = p_n(K^-) \tag{2.1}$$

$$p_n(K) = p_n(K^+) + p_n(K^-) = 2p_n(K^+). \tag{2.2}$$

While this is quite straight-forward, the situation becomes a little confusing when compounded knots are considered. For example, the knot $3_1^+\#3_1^-$ is achiral, but $3_1^+\#3_1^+$ is chiral. Since we will study both left and right handed-versions of chiral knots, it is convenient to define

$$p_n^{\pm}(K) = \begin{cases} p_n(K) & \text{if } K \text{ is achiral} \\ p_n(K^+) + p_n(K^-) & \text{if } K \text{ is chiral} \end{cases}. \tag{2.3}$$

So, for example, for the left and right handed granny knots we have

$$p_n^{\pm}(3_1^+\#3_1^+) = p_n(3_1^+\#3_1^+) + p_n(3_1^-\#3_1^-) = 2\,p_n(3_1^+\#3_1^+). \tag{2.4}$$

Note that the above does not enumerate any polygons of the achiral knot type $3_1^+\#3_1^-$ (this is the *square knot*). An additional example of this definition for com-

pounded right and left-handed trefoil is

$$p_n^{\pm}(3_1^+\#3_1^+\#3_1^-) = p_n(3_1^+\#3_1^+\#3_1^-) + p_n(3_1^-\#3_1^-\#3_1^+). \tag{2.5}$$

Generally, define $p_n^{\pm}(K)$ as follows:

$$p_n^{\pm}(K) = \begin{cases} p_n(K^+) + p_n(K^-), & \text{if } K \text{ is chiral;} \\ p_n(K), & \text{if } K \text{ is achiral.} \end{cases} \tag{2.6}$$

It follows for example that $p_n^{\pm}(4_1) = p_n(4_1)$ while $p_n^{\pm}(3_1) = p_n(3_1^+) + p_n(3_1^-)$.

2.1. *Minimal Knotted Polygons*

In order for the GAS algorithm to estimate $p_n(K)$ for a range of n, we need to know this number exactly for at least one specific value of n. For convenience we compute the number of polygons of minimal length for a given knot type. In the case of unknotted polygons, we have $p_4(0_1) = 3$.

For each knot type K there is a number $n_{min}(K)$ such that $p_n(K) = 0$ if $n < n_{min}(K)$ and otherwise $p_n(K) > 0$ for even n. The number $n_{min}(K)$ is the minimal length of the knot type K in the cubic lattice [21,15]. The number of polygons of this knot-type and minimal length is $p_{n_{min}(K)}(K)$.

Some care should be taken when K is chiral knot. The minimal length does not depend on the handedness of the knot and as noted above $p^{\pm}_{n_{min}(K)}(K) = p_{n_{min}(K)}(K^+) + p_{n_{min}(K)}(K^-) = 2\,p_{n_{min}(K)}(K^+)$.

In the case of the trefoil knot, it has been proven that $n_{min}(3_1) = 24$ [6] and $p_{24}^{\pm}(3_1) = 3328$ [7,42]. Thus, it follows that $p_n(3_1^+) = 1664$. Each embedding of a minimal trefoil knotted polygon (of length 24) in the cubic lattice can be rotated and reflected into other conformations by the 24 elements of the octahedral group. In most cases this gives 24 distinct polygons of knot types 3_1^+ and 3_1^-. However, since 3328 is not a multiple of 24 it follows that there are minimal trefoils that are symmetric under rotations in the cubic lattice.

This observation applies to other knot types. Each polygon may be reflected and rotated by the elements of the octahedral group, defining a symmetry class of polygons equivalent under these rotations and reflections. Most equivalence classes obtained in this way will have 24 distinct elements. There are exceptions to this. For example, the minimum length unknotted polygons of length 4 all belongs to a symmetry class with just 3 distinct members. In the case of the trefoil, our simulations show that there are 142 distinct symmetry classes of minimal length polygons of length 24 edges.

The figure eight knot 4_1 is achiral, and it is known that $n_{min}(4_1) = 30$ and $p_{30}(4_1) = 3648$ [42]. Reflections and rotations of figure eight knots by the elements of the octahedral group similarly gives equivalence classes, and our simulations will show that there are 278 distinct equivalence classes for this knot. Observe that $278 \times 24 = 3648$ so that each equivalence class contains 24 members, and every

embedded minimal length figure eight knot has 24 distinct images under reflections and rotations in the cubic lattice.

2.2. *Amplitude Ratios of Knotted Polygons*

There are considerable numerical evidence that

$$p_n^{\pm}(K) \simeq C_K n^{\alpha-3+N_K} \mu_{0_1}^n \tag{2.7}$$

so that the entropic exponent of polygons of knot type K is given by $\alpha_K = \alpha + N_K$ where N_K is the number of prime components in the knot type K and α is the entropic exponent of lattice polygons. This form for $p_n(K)$ was already conjectured in reference [35]; see reference [38] for more results, and also reference [32] for strong numerical evidence for this this ansatz.

Since $p_n(3_1) = 0$ if $n < 24$ and $p_{24} = 3328$, it is known that $p_n(0_1) > p_n(3_1)$ for small even values of n. Non-rigorous arguments based on a pattern theorem for knotted polygons (see reference [44]) and equation (2.7) strongly suggest that there exists a least integer $M_{0_1,3_1}$ such that

$$p_n(0_1) \leq p_n^{\pm}(3_1), \quad \text{for all even } n \geq M_{0_1,3_1}. \tag{2.8}$$

Since $p_n^{\pm}(3_1) = 0$ if $n < 24$, it follows that $p_n(0_1) > p_n^{\pm}(3_1)$ for small values of n, and there is a crossover at $n = M_{0_1,3_1}$ where trefoils begin to dominate unknotted polygons in the ensemble of lattice polygons.

In this paper we estimate $M_{0_1,3_1}$ by examining amplitude ratios. Taking ratios of equation (2.7) with $K = 0_1, N_K = 0$ and $K = 3_1, N_K = 1$ gives

$$\frac{n\, p_n(0_1)}{p_n^{\pm}(3_1)} \simeq \left[\frac{C_{0_1}}{C_{3_1}}\right] \qquad \text{as } n \to \infty. \tag{2.9}$$

where $[C_{0_1}/C_{3_1}]$ is an *amplitude ratio*. If we now set $n = M_{0_1,3_1}$, and assume that we also have $p_n(0_1) \approx p_n(3_1)$, then

$$M_{0_1,3_1} \approx \left[\frac{C_{0_1}}{C_{3_1}}\right]. \tag{2.10}$$

Therefore, the amplitude ratio estimates $M_{0_1,3_1}$, and by measuring the ratio we can estimate when there is a change in dominance from the number of unknots to trefoils in the ensemble of cubic lattice polygons. In other words,

$$p_n(0_1) \begin{cases} \gtrsim p_n^{\pm}(3_1) & \text{if } n \leq M_{0_1,3_1}, \\ \lesssim p_n^{\pm}(3_1) & \text{if } n \geq M_{0_1,3_1}. \end{cases} \tag{2.11}$$

Observe that if $p_n^{\pm}(3_1)$ is replaced by $p_n(3_1^+)$ in the above, then equation (2.9) becomes

$$\frac{n\, p_n(0_1)}{2\, p_n(3_1^+)} \simeq \left[\frac{C_{0_1}}{C_{3_1}}\right] \qquad \text{as } n \to \infty. \tag{2.12}$$

and a similar argument shows

$$M_{0_1,3_1^+} = 2\, M_{0_1,3_1}. \tag{2.13}$$

Thus doubling $M_{0_1,3_1}$ will give an estimate of the length at which one partner in the chiral pair of knots will start to dominate the unknot. Thus, if polygons of trefoil knot type (left- or right-handed) start to dominate unknotted polygons at $n \approx M_{0_1,3_1}$, then right-handed (or left-handed) trefoils will begin to dominate unknots at $n \approx M_{0_1,3_1^+} = 2\, M_{0_1,3_1}$.

More generally, if we take ratios of equation (2.7) for arbitrary given knot types K and L, we define the amplitude ratio $M_{K,L}$ by

$$M_{K,L} \approx \begin{cases} \left[\frac{C_K}{C_L}\right]^{1/(N_L - N_K)} & \text{if } N_L > N_K; \\ \left[\frac{C_K}{C_L}\right] & \text{if } N_L = N_K. \end{cases} \tag{2.14}$$

When $N_K > N_L$, then $M_{L,K}$ can be defined by noting that $M_{L,K} = 1/M_{K,L}$.

If $N_K = N_L$ then it follows that

$$p_n^{\pm}(K) \simeq [M_{K,L}] p_n^{\pm}(L), \quad \text{as } n \to \infty. \tag{2.15}$$

so that $M_{K,L}$ is the relative asymptotic frequency of knot types K and L. On the other hand, if $N_L > N_K$, then it follows from equation (2.14) that $p_n^{\pm}(K) \approx p_n^{\pm}(L)$ when $n \approx M_{K,L}$. In other words, $M_{K,L}$ is an estimate of the lengths where knotted polygons of type L becomes more numerous than knotted polygons of type K. That is,

$$p_n^{\pm}(K) \begin{cases} \gtrsim p_n^{\pm}(L), & \text{if } n \le M_{K,L}; \\ \lesssim p_n^{\pm}(L), & \text{if } n \ge M_{K,L}, \end{cases} \tag{2.16}$$

so that $M_{K,L}$ approximates the length at which $p_n^{\pm}(L)$ starts to dominate $p_n^{\pm}(K)$.

3. GAS Sampling of Knotted Polygons

Let ω be a cubic lattice polygon of length n. Three successive edges in ω forming a $\sqcup$-conformation outline a *negative atmospheric plaquette* incident with the polygon. On the other hand, if an edge in ω can be replaced by three edges in a $\sqcup$-conformation to create a polygon of length $n+2$, then these edges outline a *positive atmospheric plaquette*. These positive and negative atmospheric plaquettes are induced by BFACF-moves of type II as shown in figure 1.

Similarly, two adjacent edges forming a right-angle and bounding a unit square containing exactly two edges and three vertices of the polygon is a *neutral atmospheric plaquette*. Such neutral atmospheric plaquettes are induced by BFACF-moves of type I as described in figure 1.

The *size* of the negative (plaquette) atmosphere of ω is denoted by $a_-(\omega)$ and is the number of negative atmospheric plaquettes along ω. We similarly define

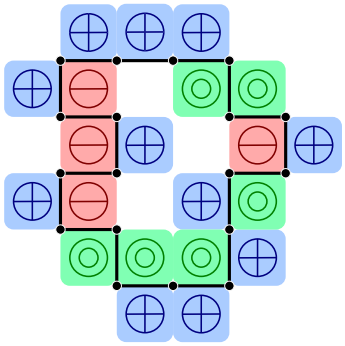

Fig. 2. Plaquette atmospheres induced by the BFACF elementary moves. This polygon has positive atmosphere $a_+ = 11$, neutral atmosphere $a_0 = 6$ and negative atmosphere $a_- = 4$.

and denote the size of the positive atmosphere, $a_+(\omega)$ and the size of the neutral atmosphere, $a_o(\omega)$. Note that $a_+(\omega), a_-(\omega)$ and $a_o(\omega)$ equivalently indicate the number of possible different length increasing, length decreasing and fixed length BFACF moves that can be performed on the current polygon ω. In figure 2 we illustrate the plaquette atmospheres of a polygon.

The GARM kinetic growth algorithm [40] can be implemented for polygons in the square lattice using the plaquette atmospheres in figure 2. This follows because it is known that by using negative (length reducing) and neutral (fixed-length) BFACF-moves, any square lattice polygon can be reduced to the minimal polygon of length 4 edges, for details, see the discussion preceding and following Theorem 2.1 in reference [19], and Theorem 9.7.2 in reference [31] for a proof.

Unfortunately, GARM based on plaquette atmospheres cannot be used to sample cubic lattice polygons, since the elementary moves of the BFACF algorithm are not irreducible on the cubic lattice polygons. This follows in particular because the knot type of a polygon cannot be changed by the moves in figure 1. Nor is it possible to sample knotted polygons of fixed knot type using GARM. This is because the shortest length polygons of any given knot type are not unique. For example there are 3 unknotted polygons of length 4, and one cannot transform one of these into the others by a sequence of neutral BFACF moves.

The GAS algorithm is a generalisation of GARM sampling to include fixed-length, length-increasing and length-decreasing moves [19]. If it is implemented with the BFACF moves described above then the following theorem shows that it is ergodic on cubic lattice polygons of fixed knot type:

Theorem 3.1 (see reference [24]). *The irreducibility classes of the BFACF moves for unrooted polygons in the cubic lattice coincide with the knot types of the polygons as closed simple curves in three dimensions.* ♢

We have implemented GAS as described in reference [19]. Polygons of knot

type K are sampled using positive, negative and neutral atmospheric moves (in our implementation these correspond to the positive, negative and neutral BFACF-moves – In other words, in the implementation of GAS in this paper, the terms "atmospheric moves" and "BFACF moves" are synonymous).

The algorithm samples along a sequence of states $\phi = \langle \phi_j \rangle = \langle \phi_0, \phi_1, \ldots, \phi_j, \ldots \rangle$ where ϕ_0 is a starting polygon of knot type K and ϕ_{j+1} is obtained from ϕ_j by executing one of the possible atmospheric moves. In this context we call ϕ_{j+1} the *successor* and ϕ_j the *predecessor*.

The precise move is chosen randomly according to the probabilities described below. These depend on a sequence of parameters β_ℓ that only depend on the length of the polygon. Given a polygon of length ℓ atmospheric moves are chosen with probabilities

$$P_+(\text{positive atmospheric move}) = \frac{\beta_\ell a_+(\phi_j)}{a_-(\phi_j) + a_0(\phi_j) + \beta_\ell a_+(\phi_j)}; \tag{3.1}$$

$$P_0(\text{neutral atmospheric move}) = \frac{a_0(\phi_j)}{a_-(\phi_j) + a_0(\phi_j) + \beta_\ell a_+(\phi_j)}; \tag{3.2}$$

$$P_-(\text{negative atmospheric move}) = \frac{a_-(\phi_j)}{a_-(\phi_j) + a_0(\phi_j) + \beta_\ell a_+(\phi_j)}. \tag{3.3}$$

Clearly if β_ℓ is large then length-increasing moves will tend to be chosen, while if it is small then fixed-length or length-reducing moves will ten to occur. Hence the sequence β_ℓ controls the average length of polygons sampled. If one chooses

$$\beta_\ell = \frac{\langle a_-(\phi) \rangle_\ell}{\langle a_+(\phi) \rangle_\ell} \tag{3.4}$$

then one balances the probability of selecting length increasing and length decreasing moves. If, in addition, $\beta_{n_{max}} = 0$ then these choices should produce roughly equal numbers of samples at all lengths $\ell < n_{max}$ of states sampled by GAS. This is the flatGAS algorithm for polygons [23].

Suppose that flatGAS has sampled along a sequence ϕ of length $|\phi|$, and with states ϕ_j of lengths ℓ_j at levels j. We associate a weight W_j with each state ϕ_j along the sequence. Define the function σ on the sequence ϕ by

$$\sigma(\phi_j, \phi_{j+1}) = \begin{cases} -1, & \text{if } \phi_{j+1} \text{ follows } \phi_j \text{ through } a_+; \\ +1, & \text{if } \phi_{j+1} \text{ follows } \phi_j \text{ through } a_-. \end{cases}$$

That is, if $\phi_j \to \phi_{j+1}$ through a positive atmospheric move, then $\sigma(\phi_j, \phi_{j+1}) = -1$, and if $\phi_j \to \phi_{j+1}$ through a negative atmospheric move, then $\sigma(\phi_j, \phi_{j+1}) = +1$. Let the weight of the first state ϕ_0 be $W_0 = 1$, and update the weights of the states W_j along the sequence by first computing

$$W'_{j+1} = \left(a^g_-(\phi_j) + a^g_0(\phi_j) + \beta_{\ell_j} a^g_+(\phi_j) \right) W_j$$

and then updating

$$W_{j+1} = \frac{W'_{j+1}\beta_{\ell_{j+1}}^{\sigma(\phi_j,\phi_{j+1})}}{\left(a_-^g(\phi_{j+1}) + a_0^g(\phi_{j+1}) + \beta_{\ell_{j+1}} a_+^g(\phi_{j+1})\right)}.$$

This produces the next state ϕ_{j+1} in the sequence ϕ with weight W_{j+1}. The weight of the sequence ϕ is given by

$$W(\phi) = \left[\frac{a_-^g(\phi_0) + a_0^g(\phi_0) + \beta_{\ell_0} a_+^g(\phi_0)}{a_-^g(\phi_L) + a_0^g(\phi_L) + \beta_{\ell_L} a_+^g(\phi_L)}\right] \prod_{j=0}^{|\phi|-1} \beta_{\ell_j}^{\sigma(\phi_j,\phi_{j+1})}. \tag{3.5}$$

It follows that the asymptotic average weight $\langle W_n\rangle$ of states of length n encountered along the sequence ϕ is proportional to the number of polygons of length n. To see this, run the process in reverse so that it terminates in the initial state ϕ_0. Then the mean conditional probability $\langle P(\phi_0|\tau)\rangle_n$ that the backwards sequence ϕ will terminate in ϕ_0, having started in a state τ becomes independent of n, since the backwards chain is an irreducible and recurrent Markov process in a finite state space. In particular, $\langle P(\phi_0|\tau)\rangle_n$ is asymptotically independent of ϕ_0 and τ. Thus if ratios of the mean accumulated weights are taken, then

$$\frac{\sum_{|\tau|=n}\langle W(\phi)\rangle_\tau}{\sum_{|\sigma|=m}\langle W(\phi)\rangle_\sigma} = \frac{p_n(K)}{p_m(K)}. \tag{3.6}$$

This means that if $p_m(K)$ is known for any value of m, then one may estimate $p_n(K)$ for $n \geq m$. Here we compute $p_{n_{min}}(K)$ for different knot types and use the above equation to estimate $p_n(K)$.

4. Numerical Results

FlatGAS simulations of knotted polygons were done in a series of runs of polygons of (even) lengths in the interval $[n_{min}(K), n_{max}(K)]$ for some convenient choice of $n_{max}(K)$ (usually equal to 2500) and where $n_{min}(K)$ is the minimal length of knot type K in the cubic lattice.

FlatGAS sequences, each of length 10^7 states were realised in this interval, and the data collected, binned at each n, and then analysed. The number of sequences is displayed in Table 1 in the column marked by "Iterations". For example, a total 2500 sequences were realised for the unknot, and 2000 sequences for trefoils. The value of $n_{max}(K)$ was put equal to 2500, except for 500 sequences in the cases marked by a (*), were $n_{max}(K) = 500$. In each case, $n_{min}(K)$ is the minimal length of the knot type K in the cubic lattice. For example, $n_{min}(0_1) = 4$ and $n_{min}(3_1) = 24$ [6].

4.1. *Estimating the number of knots of minimal length*

In order to estimate $p_n^{\pm}(K)$ using equation (3.6), we need to know the number of polygons of a given knot type at a particular length; it is arguably easiest to use the

Table 1. Knotted Polygons of Minimal Length.

K	$n_{min}(K)$	$p^{\pm}_{n_{min}}(K)$	Symmetry classes	Iterations ($\times 10^7$)
0_1	4	3	1	2500*
3_1^+	24	3328	142	2000*
4_1	30	3648	152	1500*
5_1^+	34	6672	278	1000*
5_2^+	36	114912	4788	500
6_1^+	40	6144	258	500
6_2^+	40	32832	1368	500
6_3	40	3552	148	500
8_{19}^+	42	13992	592	500
$3_1^+\#3_1^-$	40	143904	6056	500
$3_1^+\#3_1^+$	40	30576	1275	500
$3_1^+\#4_1$	46	359712	14988	500
$4_1\#4_1$	52	334824	13987	500
$3_1^+\#3_1^+\#3_1^+$	56	288816	12034	500
$3_1^+\#3_1^+\#3_1^-$	56	8874648	369777	500
$3_1^+\#3_1^+\#3_1^+\#3_1^+$	72	2752304	114680	500

shortest possible length for each knot type. These numbers have been computed independently [42] using a similar method.

The number $p^{\pm}_{n_{min}}(K)$ was estimated by sieving all minimal knots as they are encountered during the simulation. These knotted polygons were put in a standard lexicographic least string, and then rotated and reflected by elements of the octahedral group to find all members of each equivalence class. These strings were then hashed and listed as they were generated. This approach proved effective for simpler knots, and produced the correct numbers for the trefoil and figure eight knots observed elsewhere (see reference [42,43]).

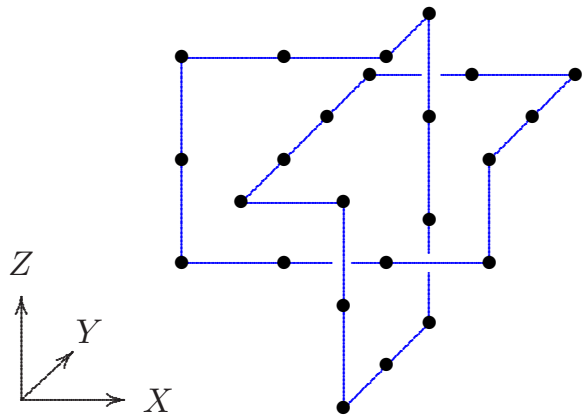

Fig. 3. A minimal length lattice trefoil knot of length 24 and with only 8 distinct conformations under rotations and reflections in the cubic lattice.

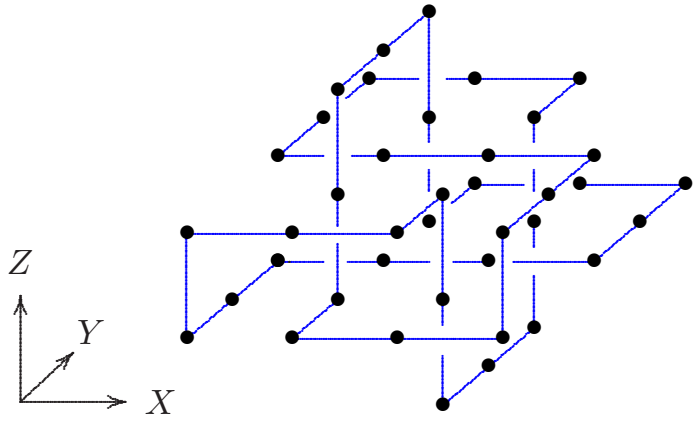

Fig. 4. A minimal length lattice knot of type 6_1 and length 40 edges and with only 12 distinct conformations under symmetry operations of the octahedral group. This particular polygon is invariant under a 180° rotation and belongs to an equivalence class with only 12 distinct members under reflections and rotation of the cubic lattice onto itself.

The results are listed in Table 1. The second and third columns list n_{min} and $p^{\pm}_{n_{min}}(K)$, while the fourth column is the number of distinct symmetry classes of knots under symmetry operations of the octahedral group of rotations and reflections in the cubic lattice; two knotted polygons are equivalent if they can be made identical under rotations and reflections. This group has 24 elements, and normally each equivalence class will contain 24 elements. There are, however, some classes with fewer than 24 polygons; for example, the equivalence class of minimal length unknotted polygons of length 4 has only three distinct members while the minimal length lattice polygon of knot type trefoil and length 24 illustrated in figure 3 has only 8 distinct rotations and reflections of itself under elements of the octahedral group and so in a symmetry class comprised of 8 distinct polygons.

In figure 4 an example of a minimal knot of type 6_1 belonging to an equivalence class with only 12 distinct members is illustrated. In general, the examples such as those in figures 3 and 4 seem to be rare. In Table 1 only the prime knot types 3_1, 6_1 and 8_{19} produced such examples. Amongst the compound knots we considered, the knot types $3_1^+\#3_1^-$, $3_1^+\#3_1^+$, $4_1\#4_1$ and $3_1^+\#3_1^+\#3_1^+\#3_1^+$ produced examples of classes with rotational or reflection symmetry.

The numbers for $p^{\pm}_{n_{min}}(K)$ and the symmetry classes in Table 1 are exact for the unknot and for the knots 3_1 and 4_1. For all the other knots, the data listed are lower bounds. While we are confident that the estimates higher up in the table are the correct values, our confidence declines as one descends the table (or as $p^{\pm}_{n_{min}}(K)$ increases in size). The most challenging cases were compounded knots with multiple components, such as $3_1^+\#3_1^+\#3_1^-$ and $3_1^+\#3_1^+\#3_1^+\#3_1^+$. The knot type $3_1^+\#3_1^+\#3_1^-\#3_1^-$ proved too much for our available hardware. Wherever possible,

Table 2. Approximate Enumeration of Trefoil Polygons with GAS.

n	$p_m(0_1)$	$p_m(3_1)$	$p_m(4_1)$
4	3		
6	22		
8	$(2.0699 \pm 0.0024) \times 10^2$		
10	$(2.4143 \pm 0.0047) \times 10^3$		
12	$(3.1863 \pm 0.0081) \times 10^4$		
14	$(4.541 \pm 0.014) \times 10^5$		
16	$(6.856 \pm 0.023) \times 10^6$		
18	$(1.084 \pm 0.0041) \times 10^8$		
20	$(1.774 \pm 0.0032) \times 10^9$		
22	$(2.987 \pm 0.015) \times 10^{10}$		
24	$(5.156 \pm 0.027) \times 10^{11}$	3328	
26	$(9.053 \pm 0.051) \times 10^{12}$	281050 ± 630	
28	$(1.618 \pm 0.010) \times 10^{14}$	$(1.4339 \pm 0.0053) \times 10^7$	
30	$(2.931 \pm 0.020) \times 10^{15}$	$(5.769 \pm 0.028) \times 10^8$	3648
32	$(5.380 \pm 0.039) \times 10^{16}$	$(2.005 \pm 0.011) \times 10^{10}$	$(5.414 \pm 0.017) \times 10^5$
34	$(9.980 \pm 0.076) \times 10^{17}$	$(6.342 \pm 0.039) \times 10^{11}$	$(4.341 \pm 0.025) \times 10^7$
36	$(1.871 \pm 0.015) \times 10^{19}$	$(1.862 \pm 0.012) \times 10^{13}$	$(2.495 \pm 0.018) \times 10^9$
38	$(3.537 \pm 0.030) \times 10^{20}$	$(5.204 \pm 0.038) \times 10^{14}$	$(1.164 \pm 0.010) \times 10^{11}$

we have compared our results with those obtained in reference [42], and found agreement [43].

One may obtain estimates for $p_n(K)$ from $p_n^{\pm}(K)$ for $n = n_{min}(K)$ by using equation (2.3). For example, we observe that since the trefoil is chiral, $2\,p_n(3_1^+) = p_n^{\pm}(3_1)$ and so $p_n(3_1^+) = 1664$. Similarly the figure eight knot is achiral giving $p_n(4_1) = p_n^{\pm}(4_1) = 3648$.

After $p_{n_{min}}(K)$ is estimated, the flatGAS data can be used to estimate $p_n(K)$ using the ratios of collected weights as in equation (3.6). Some data for the unknot, the trefoil and the figure eight knot are listed in Table 2. Observe that series for all polygons is known to $n = 32$ [4] and that a comparison (for $n < 24$ before the first trefoils appear) shows that flatGAS gives good estimates: For example, $p_{18}(0_1) = 108088232$ and $p_{22}(0_1) = 29764630632$, close to the estimates in Table 2.

4.2. *Estimating* $M_{K,L}$

We now turn to the problem of estimating the amplitude ratios of different knot types described by equations (2.10) and (2.14). Our data for the unknot and the trefoil can be used to estimate $M_{0_1,3_1}$ as follows: Take the logarithm of equation (2.9) to see that

$$\log\left[\frac{n\,p_n(0_1)}{p_n^{\pm}(3_1)}\right] = \log\left[\left[\frac{C_{0_1}}{C_{3_1}}\right](1 + o(1))\right] \tag{4.1}$$

Assuming that the $o(1)$ term is approximated by C/n, we obtain from the above the approximate expression

$$\log\left[\frac{n\,p_n(0_1)}{p_n^{\pm}(3_1)}\right] \approx \log\left[\frac{C_{0_1}}{C_{3_1}}\right] + \log\left(1 + \frac{c}{n}\right) + \ldots = \log\left[\frac{C_{0_1}}{C_{3_1}}\right] + \frac{c_1}{n} + \frac{c_2}{n^2} + \ldots \tag{4.2}$$

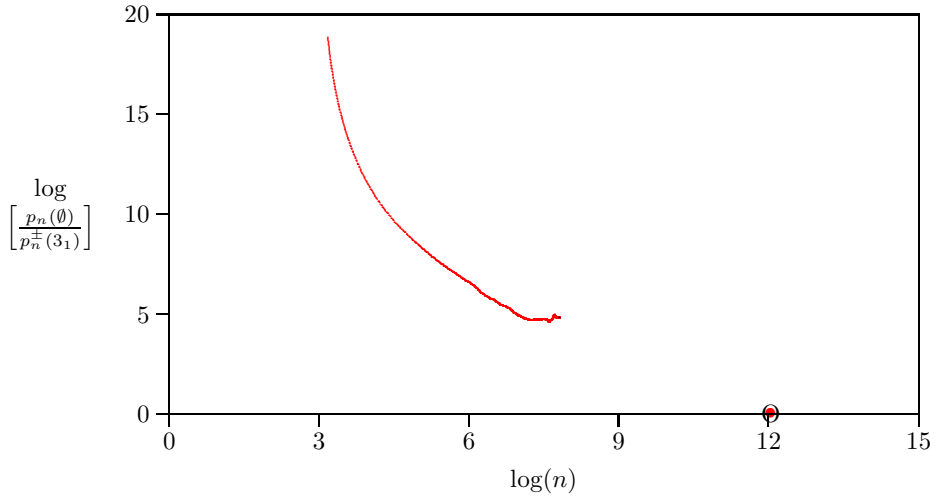

Fig. 5. The ratio $[p_n(0_1)/p_n^{\pm}(3_1)]$ as a function of length n on logarithmic scales. For small values of n, $p_n(0_1) > p_n^{\pm}(3_1)$, but since this relation changes to $p_n(0_1) < p_n^{\pm}(3_1)$ for large values of $n \geq M_{0_1,3_1}$, it must cut through the X-axis if it is extrapolated. Extrapolation of the data shows that this occurs near $\log n \approx 12.041 \pm 0.038$ (see the text for details about the extrapolation).

In other words, a three parameter regression of $\log\left[\frac{n\,p_n(0_1)}{p_n^{\pm}(3_1)}\right]$ against the model $c_0 + c_1/n + c_2/n^2$ should produce an estimate of $c_0 = \left[\frac{C_{0_1}}{C_{3_1}}\right] = M_{0_1,3_1}$.

More generally, estimates of $M_{K,L}$ for knots of types K and L, can be obtained by considering the model

$$\begin{aligned}\log\left[\frac{n^{-N_K}\,p_n^{\pm}(K)}{n^{-N_L}p_n^{\pm}(L)}\right] &\approx \log\left[\frac{C_K}{C_L}\right] + \log\left(1+\frac{c}{n}\right) + \dots \\ &= \log\left[\frac{C_K}{C_L}\right] + \frac{c_1}{n} + \frac{c_2}{n^2} + \dots \end{aligned} \tag{4.3}$$

where one may replace $p_n^{\pm}(K)$ by $p_n(K)$ or $p_n^{\pm}(L)$ by $p_n(L)$, or both (leading to similar changes to C_K and C_L). Thus, if $p_n^{\pm}(K) = p_n^{\pm}(L)$ then $n = M_{K,L}$ can be determined by solving for $M_{K,L}$ in equation (2.14). Since $M_{K,L} = 1/M_{L,K}$, assume that L is the more complex knot (higher crossing number, more prime components) than K and so we will in most cases orient the knots such that $M_{K,L} \geq 1$. Finally, it is trivially the case that $M_{K,K} = n_{min}(K)$. One can similarly determine $M_{K,L}$ in cases that $N_L > N_K \geq 0$ by assuming that $M_{K,L}$ is large and then truncating the series on the right hand side of equation (4.3) at c_2/n^2 before solving for $M_{K,L}$ (using a linear least squares analysis).

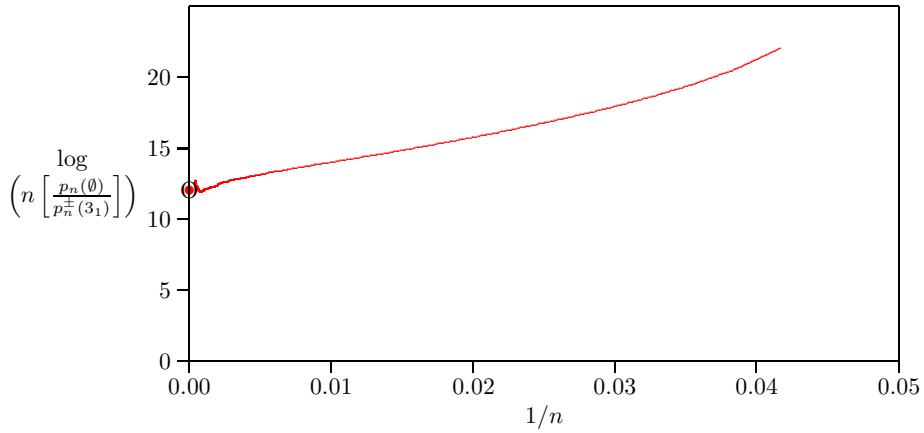

Fig. 6. Testing the hypothesis that $N_{3_1} = 1$ for the trefoil knot in equation (2.7). The data approaches a non-zero constant as $n \to \infty$, and the value of this Y-intercept is an estimate of the amplitude ratio $[C_{0_1}/C_{3_1}]$. These data also give the estimate $M_{0_1,3_1} = 170000 \pm 12000$ so that $p_n(0_1) \approx p_n^{\pm}(3_1)$ when $n \approx M_{0_1,3_1}$ and $p_n(0_1) < p_n(3_1)$ for $n > M_{0_1,3_1}$. In other words, polygons of knot type trefoil start to dominate unknotted polygons at lengths of about 170000 edges.

4.3. *The Unknot and the Trefoil*

Let us now focus on the results for the unknot and the trefoil. In Table 2 we give some small-n estimates from our flatGAS simulations. These suggest that for small values of n, $[p_n(0_1)/p_n^{\pm}(3_1)] > 1$. The conjectured asymptotic behaviour of $p_n^{\pm}(3_1)$ given by equation (2.7) with $N_{3_1} = 1$ implies that $p_n^{\pm}(3_1)$ will exceed $p_n(0_1)$ for large values of n. There is evidence of this in the literature; see for example [35]. Thus, for large values of n, the relationship inverts to $[p_n(0_1)/p_n^{\pm}(3_1)] < 1$ and trefoil polygons become more numerous than unknotted polygons. As described above, the cross over occurs at $n \approx M_{0_1,3_1}$.

In figure 5 we graph $\log[p_n(0_1)/p_n^{\pm}(3_1)]$ against $\log n$. With increasing values of n, the curve decreases, and since $[p_n(0_1)/p_n^{\pm}(3_1)] < 1$ if $n > M_{0_1,3_1}$, the curve should cut through the X-axis when $n \approx M_{0_1,3_1}$. Hence we estimate of $M_{0_1,3_1}$ by fitting the data in this figure to the model in equation (4.3) using a weighted least squares model. This extrapolates the curve to its intersection with the X-axis in the figure; we have indicated this estimate with a bullet.

This analysis is predicated on the assumption that $N_{3_1} = 1$ in equation (2.7). We have tested this assumption by plotting $[n\, p_n(0_1)/p_n^{\pm}(3_1)]$ against $1/n$. This curve should approach a constant (non-zero) intercept with the Y-axis as $n \to \infty$ (see equation (2.9)). We have plotted $\log[n\, p_n(0_1)/p_n^{\pm}(3_1)]$ against $1/n$ in figure 6. This clearly shows that the data approaches a point between 10 and 15 on the Y-axis with increasing n. This is strong numerical evidence that $N_{3_1} = 1$.

The value of the Y-intercept in figure 6 is exactly that of the X-intercept in figure 5 and is equal to $\log[C_{0_1}/C_{3_1}]$. We have determined it by fitting our data to

equation (4.2) using a three parameter weighted least squares linear regression of the data in figure 6. We tracked the least squared error as a goodness-of-fit parameter; this is distributed as a χ^2-statistic. The regression improved when data points at both the smallest values of n (where there are strong corrections to the model) and at the largest values of n (where the statistical uncertainties in the data are largest) were discarded. In general, our data were best modeled by rejecting points from $n > 1500$ edges, so that we assumed $n \in [n_{min}(K), 1500]$, and then performed regressions by discarding points for $n = n_{min}(K), n_{min}(K) + 2, n_{min}(K) + 4, \ldots$.

Discarding these data at small values of n eventually gives a regression acceptable at the 95%-level. We take this as our best estimate. We determined a systematic error by incrementing n from its minimum value by 2 again, and then taking the absolute difference in our results. This produces in general a systematic error in size comparable to the 95% statistical error. The combined errors will give our confidence interval

The results for the data in figure 6 was as follows: An acceptable regression is obtained with $n_{min} = 34$ and $n_{max} = 1500$. For this fit, $\chi^2 \approx 757$ on 732 degrees of freedom, acceptable at the 75%-level. This gives $\log[C_{0_1}/C_{3_1}] = 12.0410 \pm 0.0074$. Incrementing n_{min} to 36 gives an acceptable regression with $\log[C_{0_1}/C_{3_1}] = 12.0159 \pm 0.0075$. Putting these together gives our best estimate for $\log M_{0_1,3_1} = \log[C_{0_1}/C_{3_1}] = 12.0410 \pm 0.0074 \pm 0.0251$, were the format is estimate $\pm$ 67%-confidence interval $\pm$ systematic error.

Exponentiating these estimates will give an estimate for $M_{0_1,3_1}$. We determine a confidence interval by combining the estimated statistical and systematic errors into a single confidence interval, and then doubling it in size again to obtain a confidence interval of size larger than the 95% statistical error bar. The result is

$$M_{0_1,3_1} = 170000 \pm 12000 \tag{4.4}$$

where we have rounded to the nearest 1000. In other words, the crossover between unknot and trefoil polygons occur near $n \approx 170000$. For values of n less than this, the ensemble of lattice polygons is dominated by polygons of knot type the unknot. For values of n larger than this, the ensemble is first dominated by polygons of knot type trefoil, and then later by polygons of other knot types. In addition, since $M_{0_1,3_1^+} = 2\, M_{0_1,3_1}$ as in equation (2.13), it follows that

$$M_{0_1,3_1^+} = 340000 \pm 24000. \tag{4.5}$$

In other words, if $n \approx 340000$, then $p_n(0_1) \approx p_n(3_1^+) = p_n(3_1^-)$. For values of $n > M_{0_1,3_1^+}$ there are more polygons of knot type 3_1^+ than there are polygons of knot type 0_1.

4.4. *The Figure Eight Knot*

A similar analysis can be done for the figure eight knot. In figure 7 $\log[p_n(0_1)/p_n(4_1)]$ is plotted against $\log n$. Again we see that curve decreases with

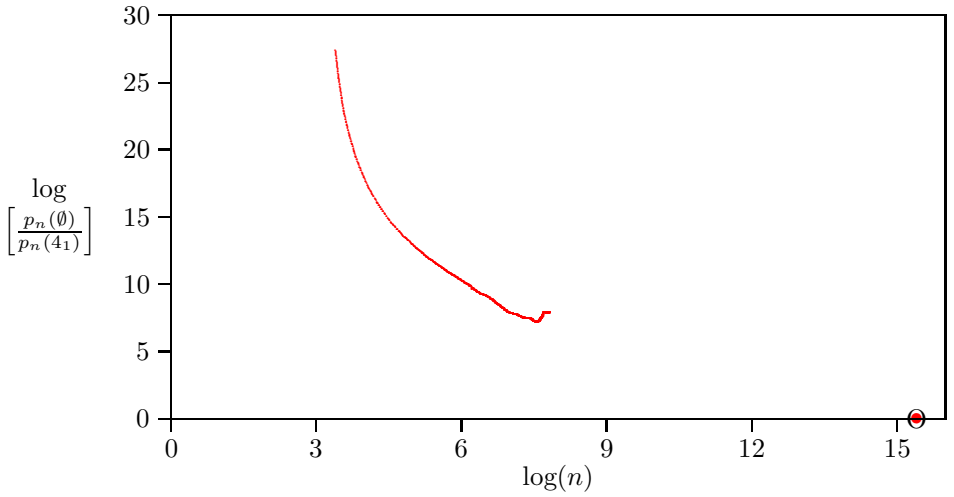

Fig. 7. The ratio $[p_n(0_1)/p_n(4_1)]$ against n on logarithmic axes. The proportion of polygons of knot type 4_1 increases relative to the number of unknotted polygons with n, and extrapolation of the curve shows that it approaches the X-axis when $\log n = 15.403 \pm 0.047$.

n showing that the ratio of figure eights to unknots is increasing. Extrapolating the data gives the X-intercept indicated by the bullet. The extrapolation was done using the same method used in figure 6, and the plot of $\log[p_n(0_1)/p_n(4_1)]$ against $1/n$ is given in figure 8. Again this plot also provides compelling evidence that $N_{4_1} = 1$.

The data in figure 8 exhibits strong corrections and we could not find a consistent estimate for $M_{0_1,4_1}$ when data with $n > 700$ is included in the regressions. Discarding data at values of $n > 700$ gave consistent results, and incrementing $n_{min} = 30$ to $n_{min} = 58$ gives an acceptable regression. The result is that $\log[C_{0_1}/C_{4_1}] = 15.4030 \pm 0.0135$ at $n_{min} = 48$ with a least squares error $\chi^2 \approx 343$ on 325 degrees of freedom, acceptable at the 76.1%-level. A further increase to $n_{min} = 50$ gives $\log[C_{0_1}/C_{4_1}] = 15.3708 \pm 0.0140$ with a least squares error $\chi^2 \approx 303$ on 324 degrees of freedom, acceptable at the 20%-level.

Putting these results together shows that $\log M_{0_1,4_1} = \log[C_{0_1}/C_{4_1}] = 15.4030 \pm 0.0135 \pm 0.0328$, were the format is estimate $\pm$ 67%-confidence interval $\pm$ systematic error. The location of this point is marked by the bullet in figures 7 and figure 8. Combining the error bars, exponentiating the estimate and doubling the confidence interval again, gives

$$M_{0_1,4_1} = (4.89 \pm 0.46) \times 10^6 \tag{4.6}$$

where the error bars have been combined to give a single confidence interval, and the estimates are rounded to the nearest 1000. This shows that the crossover between the unknot and the figure eight knot occurs near $n \approx 4890000$.

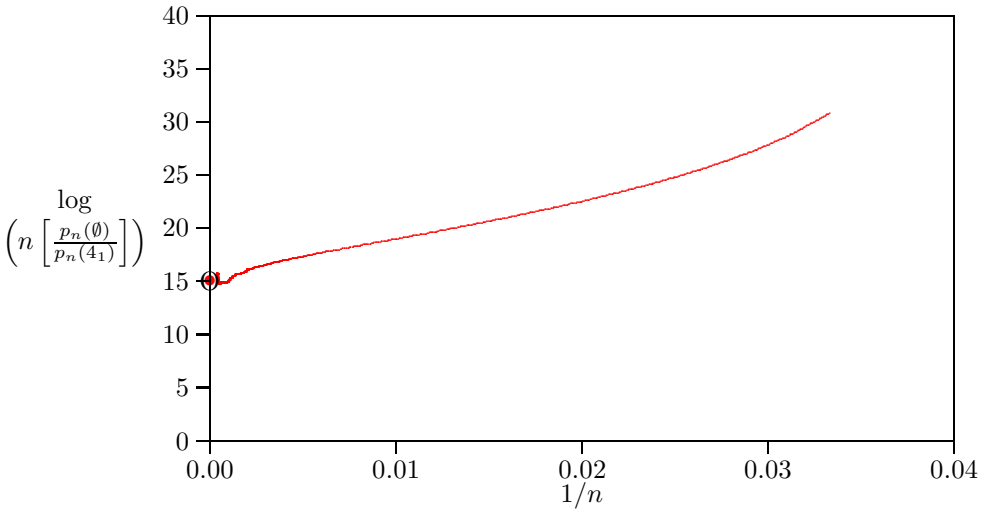

Fig. 8. Extrapolation of the data in figure 7. The curve approaches a non-zero constant as $n \to \infty$ on the Y-axis, providing strong numerical evidence that $N_{4_1} = 1$ in equation (2.7) for the figure eight knot. The amplitude ratio $[C_{0_1}/C_{4_1}]$ is estimated by the Y-intercept, and is an estimate also of $M_{0_1,4_1} = (4.89 \pm 0.46) \times 10^6$. Thus, the unknot and the figure eight knot turn over at his length.

Comparison to equation (4.4) shows that $M_{0_1,4_1} > M_{0_1,3_1}$. That is, polygons of knot type 4_1 begin to dominate unknotted polygons at much larger lengths than the crossover between unknotted polygons and trefoils. This observation implies that figure eight knots are rarer than trefoils, and that this should persist for all values of n.

We can examine this hypothesis by considering the ratio $[p_n^{\pm}(3_1)/p_n(4_1)]$. Since $N_{3_1} = N_{4_1} = 1$ in equation (2.14), plot $\log[p_n^{\pm}(3_1)/p_n(4_1)]$ against $1/n$ as in figure 9. We observe that this ratio does indeed approach a positive constant, confirming that trefoils remain more numerous than figure eights. Extrapolating this data to Y-axis gives an estimate of $M_{3_1,4_1}$.

A linear least-square regression of the data in figure 9 gives an acceptable fit for $n_{max} = 1000$ and $n_{min} = 40$. This fit gives $\log[C_{3_1}/C_{4_1}] = 3.2967 \pm 0.0098$, with $\chi^2 \approx 435$ acceptable at the 73.1%-level on 479 degrees of freedom.

Incrementing $n_{min} = 42$ gives $\log[C_{3_1}/C_{4_1}] = 3.2665 \pm 0.0101$. Comparison of these results show that $\log[C_{3_1}/C_{4_1}] = 3.2967 \pm 0.0098 \pm 0.0302$. Finally, exponentiating these estimates and doubling the combined confidence interval gives

$$M_{3_1,4_1} = 27.0 \pm 2.2. \tag{4.7}$$

This result implies that trefoil polygons are asymptotically 27.0 ± 2.2 times as abundant as figure eight polygons. These results are similar to results reported in reference [17], where the relative frequencies of figure eight and trefoil knot types in

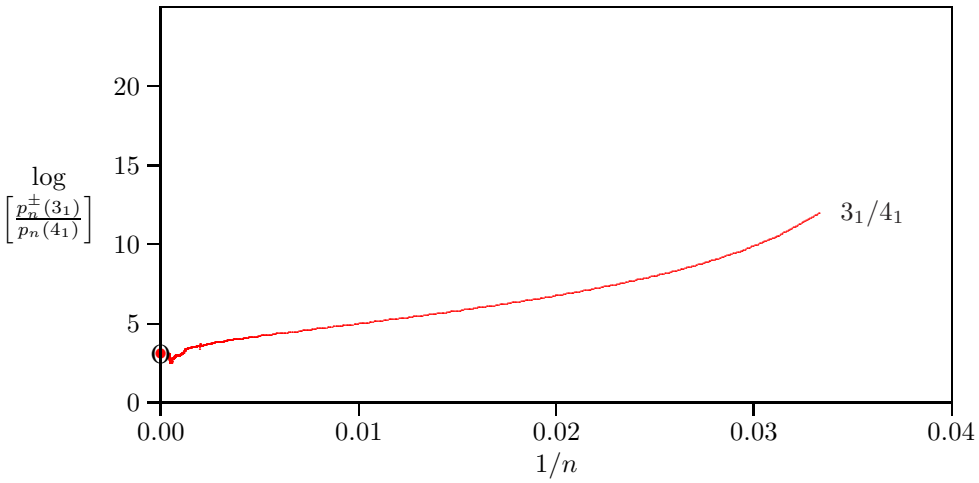

Fig. 9. Plotting $\log[p_n^{\pm}(3_1)/p_n(4_1)]$ against n to determine the asymptotic relative frequency of trefoils and figure eights in polygons. Extrapolation to the Y-axis shows that $M_{3_1,4_1} = 27.0 \pm 2.2$; in other words, for every 27 trefoils, we should observe one figure eight knot in the limit of large n.

polygons were estimates using a different approach based on knotting probabilities in random self-avoiding polygons. Observe that $M_{0_1,3_1} \times M_{3_1,4_1} \approx 4.59 \times 10^6$ and that this is comparable to $M_{0_1,4_1} = (4.89 \pm 0.46) \times 10^6$. Since $p_n^{\pm}(3_1) = 2\,p_n(3_1^+)$, it also follows that $M_{3_1^+,4_1} \approx 13.5 \pm 1.1$.

4.5. *Results for Polygons of Prime Knot Types*

We have also used flatGAS to collect data for the two five crossing prime knots 5_1 and 5_2, the three six crossing prime knots 6_1, 6_2 and 6_3, and for the (first) non-alternating prime knot 8_{19}.

In figure 10 we plot $\log[np_n(0_1)/p_n^{\pm}(K)]$ against $1/n$ for the knots $K = 3_1, 4_1, 5_1$ and 5_2. Extrapolating to $n = \infty$ again produced estimates for $M_{0_1,K}$. Discarding data for $n > n_{max} = 1800$ and using the three parameter model in equation (4.3) gives acceptable fits for 5_1 and 5_2 for $n_{min} = 36$ and 64 respectively.

In the case of 5_1 we estimate that $\log[C_{0_1}/C_{5_1}] = 17.8362 \pm 0.0314$ for $n_{min} = 36$ with $\chi^2 \approx 42$ acceptable atthe 0% level on 331 degrees of freedom. Increasing n_{min} to 38 gives $\log[C_{0_1}/C_{5_1}] = 17.8057 \pm 0.0325$ with $\chi^2 \approx 34$ acceptable at the 0% level on 330 degrees of freedom. Comparing these to estimate the systematic error produced our best estimate $\log[C_{0_1}/C_{5_1}] = 17.8362 \pm 0.0314 \pm 0.0305$. Combining the error bars, exponentiating the estimate and doubling the confidence interval again, gives

$$M_{0_1,5_1} = (5.58 \pm 0.70) \times 10^7. \tag{4.8}$$

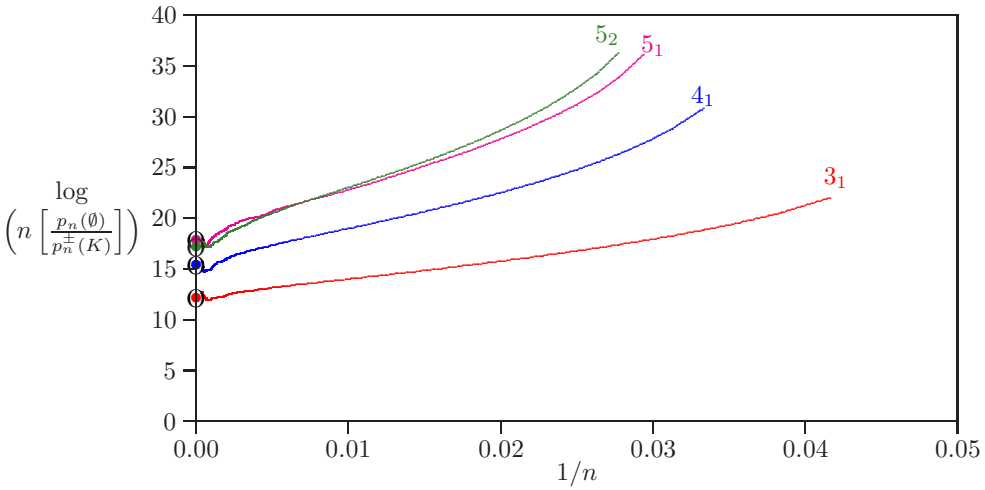

Fig. 10. $\log[np_n(0_1)/p_n^{\pm}(K)]$ plotted against $1/n$ for $K = 3_1$, 4_1, 5_1 and 5_2. In each case the curves approach a non-zero finite value as n increases, providing numerical evidence that $N_K = 1$ in equation (2.7) for these knot types. Extrapolation of the data to the Y-axis gives the points indicated by bullets. These points provide estimates of $M_{0_1,K}$ of each of the knot types.

In the case of 5_2 we estimate that $\log[C_{0_1}/C_{5_2}] = 17.1412 \pm 0.0187$ for $n_{min} = 64$ with $\chi^2 \approx 328$ acceptable at the 68% level on 317 degrees of freedom. Increasing n_{min} to 66 gives $\log[C_{0_1}/C_{5_1}] = 17.1044 \pm 0.0191$ with $\chi^2 \approx 291$ acceptable at the 16% level on 316 degrees of freedom. Comparing these to estimate the systematic error produced our best estimate $\log[C_{0_1}/C_{5_1}] = 17.1412 \pm 0.0187 \pm 0.0368$. Combining the error bars, exponentiating the estimate and doubling the confidence interval gives

$$M_{0_1,5_2} = (2.78 \pm 0.32) \times 10^7. \tag{4.9}$$

In other words, the knot 5_2 crosses over the unknot near $(2.78 \pm 0.32) \times 10^7$ before 5_1 crosses over the unknot at $(5.58 \pm 0.70) \times 10^7$. In a similar way we have estimated $M_{0_1,K}$ for six crossing knots and the results are given in Table 3.

Table 3. $M_{0_1,K}$ **for prime knots.**

$0_1/K$	$M_{0_1,K}$	$0_1/K$	$M_{0_1,K}$
3_1	$(1.70 \pm 0.12) \times 10^5$	6_1	$(6.42 \pm 0.64) \times 10^8$
4_1	$(4.89 \pm 0.46) \times 10^6$	6_2	$(7.28 \pm 0.74) \times 10^8$
5_1	$(5.58 \pm 0.70) \times 10^7$	6_3	$(1.54 \pm 0.22) \times 10^9$
5_2	$(2.78 \pm 0.32) \times 10^7$	8_{19}	$(2.78 \pm 0.28) \times 10^{10}$

One may similarly compute the amplitude ratios $M_{3_1,5_1}$, $M_{3_1,5_2}$, $M_{4_1,5_1}$, $M_{4_1,5_2}$ and $M_{5_1,5_2}$ of these prime knot types. The ratios are plotted in figure 11. The

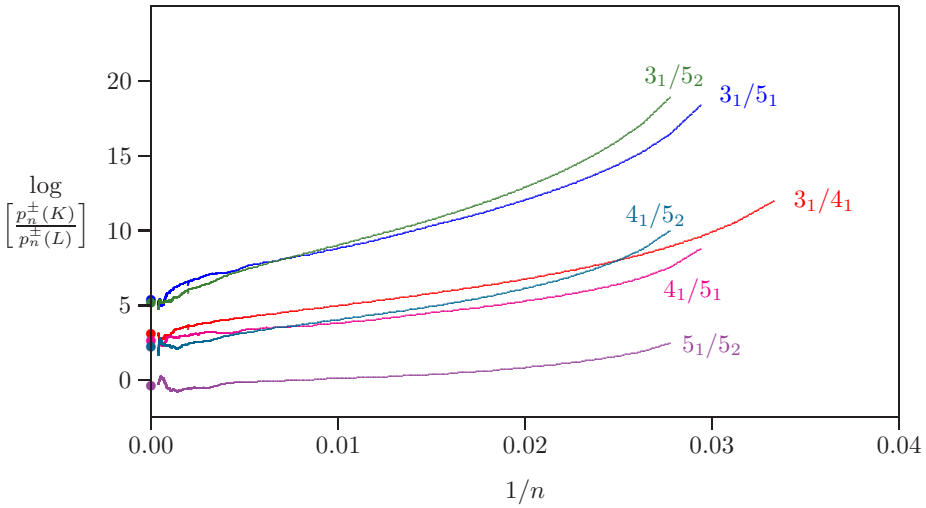

Fig. 11. Plotting $\log[p_n^{\pm}(K)/p_n^{\pm}(L)]$ against n to determine the asymptotic relative frequency of knots of types K and L in polygons.

data are quite noisy for $n > 1000$, thus we chose $n_{max} = 1000$ in our analysis and obtained the results in table 4. Observe that these results are internally consistent within twice the stated confidence intervals. For example, $M_{3_1,4_1} \times M_{4_1,5_1} = 438 \pm 76$ while $M_{3_1,5_1} = 399 \pm 44$.

Table 4. $M_{K,L}$ for prime knots ($M_{L,K} = 1/M_{K,L}$).

K/L	$M_{K,L}$	K/L	$M_{K,L}$
$3_1/4_1$	27.0 ± 2.2	$5_1/6_1$	10.8 ± 1.8
$3_1/5_1$	399 ± 44	$5_1/6_2$	11.8 ± 1.2
$3_1/5_2$	216 ± 24	$5_1/6_3$	22.2 ± 2.7
$3_1/6_1$	5160 ± 560	$5_1/8_{19}$	447 ± 56
$3_1/6_2$	6240 ± 600	$5_2/6_1$	31.0 ± 5.0
$3_1/6_3$	11900 ± 1800	$5_2/6_2$	34.6 ± 4.6
$3_1/8_{19}$	225100 ± 28000	$5_2/6_3$	71 ± 18
$4_1/5_1$	16.2 ± 1.5	$5_2/8_{19}$	1280 ± 170
$4_1/5_2$	9.0 ± 1.2	$6_1/6_2$	1.05 ± 0.13
$4_1/6_1$	218 ± 30	$6_1/6_3$	1.83 ± 0.30
$4_1/6_2$	258 ± 28	$6_1/8_{19}$	47.0 ± 5.2
$4_1/6_3$	475 ± 72	$6_2/6_3$	2.06 ± 0.32
$4_1/8_{19}$	9000 ± 1100	$6_2/8_{19}$	40.3 ± 4.6
$5_1/5_2$	0.417 ± 0.040	$6_3/8_{19}$	25.5 ± 6.4

A similar set of calculations for six crossing prime knots gives more data of this kind, and we also list these results in Table 4. Observe that ratio for one chiral partner of chiral knot types can be obtained by multiplication or dividing by a factor of two. For example, if K and L are chiral knot types, then $M_{K^+,L^+} =$

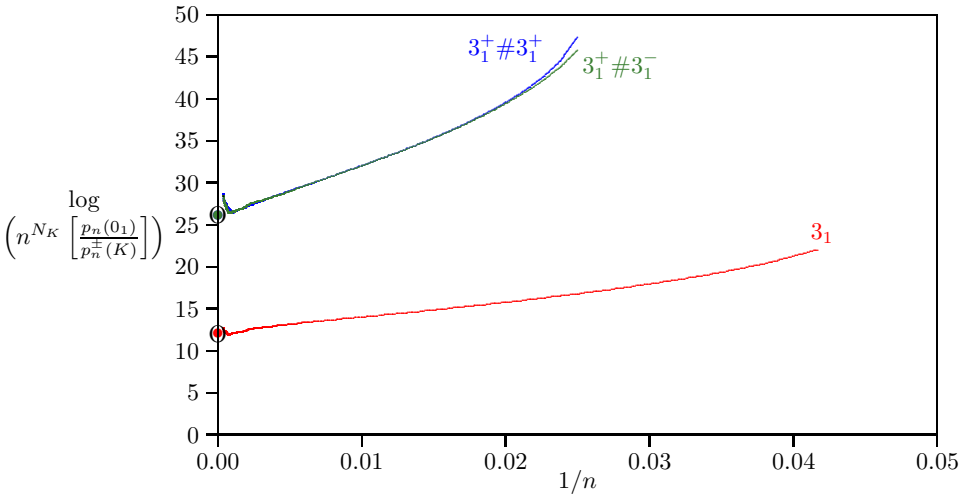

Fig. 12. Extrapolating data for knots of type $3_1^+\#3_1^+$ and $3_1^+\#3_1^-$ to estimate $M_{0_1,(3_1^+\#3_1^+)}$ and $M_{0_1,(3_1^+\#3_1^+)}$. Also plotted are data for $K = 3_1$ for comparison.

$M_{K,L} = 2\,M_{K^+,L} = 0.5\,M_{K,L^+}$. Thus, one may check that $M_{4_1,5_1^+} = 32.4 \pm 3.0$ and $M_{5_1^+,6_1} = 5.4 \pm 0.9$.

5. Numerical Results for Compound Knot Types

In this section we shift our attention to compound knots. We start by considering knots of types $3_1^N \equiv 3_1\#3_1\#3_1\#\ldots$, and then compare these to knots of type $3_1\#4_1$ and $4_1\#4_1$.

In figure 12 we plot ratio data comparing unknots to the knots 3_1, $3_1^+\#3_1^+$ and $3_1^+\#3_1^-$. An estimate for $M_{0_1,3_1}$ was already obtained in equation (4.4). In the other two cases we must set $N_{3_1^2} = 2$ in equations (2.7) and (2.14) in order to extract estimates of $M_{0_1,K}$.

In the case that $K = 3_1^+\#3_1^+$ we can compute the limiting ratio of $n^2 p_n(0_1)/p_n^{\pm}(3_1^+\#3_1^+)$ (and we remind the reader that $p_n^{\pm}(3_1^+\#3_1^+) = p_n(3_1^+\#3_1^+) + p_n(3_1^-\#3_1^-)$. A three parameter linear regression assuming the model in equation (4.3) gives the result $\log[C_{0_1}/C_{3_1^+\#3_1^+}] = 26.199 \pm 0.016 \pm 0.050$ with $n_{max} = 700$ and $n_{min} = 50$. The least square error is $\chi^2 \leq 316$ acceptable at the 40% level on 323 degrees of freedom. Taking into account that this ratio is computed from $p_n^{\pm}(3_1^+\#3_1^+)$ gives the result

$$M_{0_1,(3_1^+\#3_1^+)} = 977000 \pm 66000, \tag{5.1}$$

where, as before, we have doubled up the confidence interval.

One may similarly compute $M_{0_1,(3_1^+\#3_1^-)}$. The regression with $n_{max} = 700$ and

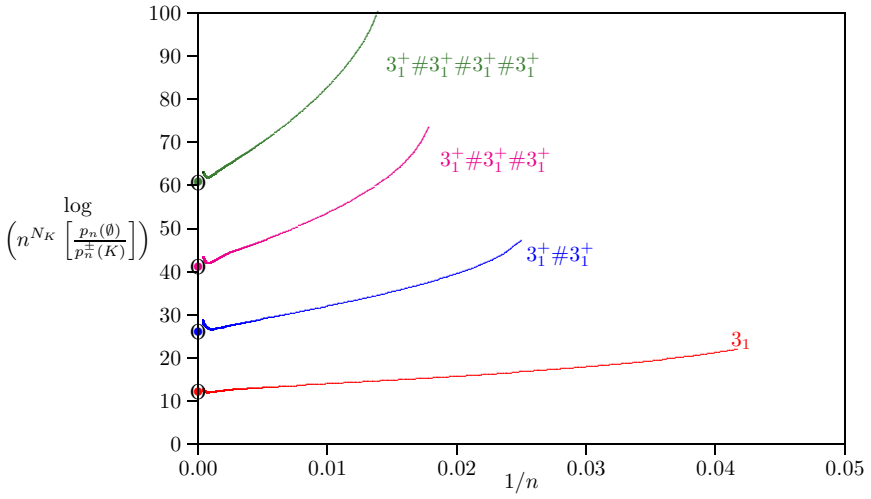

Fig. 13. Extrapolating data for compounded knots of type $(3_1^+)^N$ for $N = 1, 2, 3, 4$.

$n_{min} = 50$ has least squares error $\chi^2 \leq 286$ on 324 degrees of freedom acceptable at the 6.4% level. The result is that $\log[C_{0_1}/C_{3_1^+\#3_1^+}] = 26.228 \pm 0.015 \pm 0.045$ so that

$$M_{0_1,(3_1^+\#3_1^-)} = 496000 \pm 30000. \tag{5.2}$$

Thus the crossover between unknotted polygons and polygons of knot types $3_1^+\#3_1^-$ occurs approximately at length 496000 edges.

The curves for the amplitude ratios of $p_n^{\pm}(3_1^+\#3_1^+)$ and $p_n(3_1^+\#3_1^-)$ are practically indistinguishable in figure 12. The relation between these knot types may be checked by computing $M_{(3_1^+\#3_1^+),(3_1^+\#3_1^-)}$. Acceptable fits with $n_{max} = 700$ and $n_{min} = 42$ are obtained, and the result is

$$M_{(3_1^+\#3_1^+),(3_1^+\#3_1^-)} = 0.535 \pm 0.066. \tag{5.3}$$

In other words, the chiral knots $3_1^+\#3_1^+$ are roughly one half times as numerous as the achiral knot $3_1^+\#3_1^-$ in the asymptotic limit. This is consistent with equations (5.1) and (5.2).

We have also computed $M_{3_1^+,3_1^+\#3_1^+}$. The regression for the ratio $[np_n^{\pm}(3_1^+)/p_n^{\pm}(3_1^+\#3_1^+)]$ using the model in equation (4.3) with $n_{min} = 48$ and $n_{max} = 700$ is acceptable at the 0% level on 325 degrees of freedom and gives $\log[C_{3_1^+}/C_{3_1^+\#3_1^+}] = 14.203 \pm 0.016 \pm 0.048$. This gives the following estimate

$$M_{3_1^+,(3_1^+\#3_1^+)} = 1473000 \pm 190000, \tag{5.4}$$

so that this compounded trefoil becomes more numerous than the prime trefoil at about 1.5 million edges.

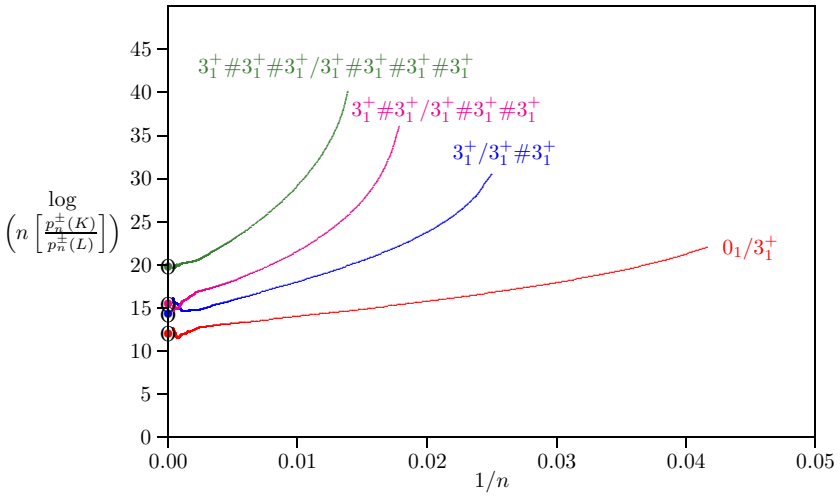

Fig. 14. Extrapolating ratios $[np_n^{\pm}((3_1^+)^{N-1})/p_n^{\pm}((3_1^+)^N]$ for $N = 1, 2, 3, 4$. In each case the curve approaches a non-zero finite constant. This is evidence that $N_{(3_1^+)^M} = M$ in equation (2.7).

We have also obtained results for the compounded knots $3_1^+\#3_1^+\#3_1^+$ and $3_1^+\#3_1^+\#3_1^+\#3_1^+$ and some of this data is plotted in figures 13 and 14. Note that $N_K = 3, 4$ respectively. The regression for the ratio $[n^3 p_n(0_1)/p_n(3_1^+\#3_1^+\#3_1^+)]$ using the model in equation (4.3) with $n_{min} = 60$ and $n_{max} = 700$ is acceptable at the 53% level on 314 degrees of freedom. It gives $\log[C_{0_1}/C_{3_1^+\#3_1^+\#3_1^+}] = 41.712 \pm 0.021 \pm 0.032$, which leads to

$$M_{0_1,(3_1^+\#3_1^+\#3_1^+)} = (2.18 \pm 0.80) \times 10^6. \tag{5.5}$$

The situation for the knot $3_1^+\#3_1^+\#3_1^+\#3_1^+$ is similar to the above. The regression for the ratio $[n^4 p_n(0_1)/p_n(3_1^+\#3_1^+\#3_1^+\#3_1^+)]$ using the model in equation (4.3) with $n_{min} = 80$ and $n_{max} = 700$ is acceptable at the 37% level on 307 degrees of freedom. It gives $\log[C_{0_1}/C_{3_1^+\#3_1^+\#3_1^+\#3_1^+}] = 61.032 \pm 0.026 \pm 0.077$ which leads to the following estimate

$$M_{0_1,(3_1^+\#3_1^+\#3_1^+\#3_1^+)} = (8.40 \pm 0.40) \times 10^6. \tag{5.6}$$

A similar analysis can be done for the ratios in figure 14 and we list these results in Table 5.

Further examination of the data above show that at a given length, compound knots of type $(3_1^+)^N$ occur with higher frequency than other compound knots. For example, a comparison of the knots $3_1^+\#3_1^+$ and $3_1^+\#4_1$ gives

$$M_{(3_1^+\#3_1^+),(3_1^+\#4_1)} = 9.4 \pm 1.2. \tag{5.7}$$

Hence knots of type $3_1^+\#3_1^+$ are roughly 9 times more numerous than knots of type $3_1^+\#4_1$ in the asymptotic limit. In addition, comparison of the knots $3_1^+\#3_1^+$ and

Table 5. $M_{K,L}$ for compounded trefoils.

$K \setminus L$	3_1^+	$(3_1^+)^2$	$(3_1^+)^3$	$(3_1^+)^4$
0_1	$3.39(23) \times 10^5$	$9.77(66) \times 10^5$	$2.18(80) \times 10^5$	$8.40(40) \times 10^6$
3_1^+	1	$1.47(19) \times 10^6$	$2.56(12) \times 10^6$	$1.245(60) \times 10^7$
$(3_1^+)^2$	—	1	$5.08(56) \times 10^6$	$3.90(28) \times 10^7$
$(3_1^+)^3$	—	—	1	$3.80(52) \times 10^8$

$4_1\#4_1$ gives

$$M_{(3_1^+\#3_1^+),(4_1\#4_1)} = 250 \pm 40, \tag{5.8}$$

so that knots of type $3_1^+\#3_1^+$ are roughly 250 times more numerous than knots of type $4_1\#4_1$ in the asymptotic limit.

Amongst polygons with knot types of the form $(3_1)^N$ (connected sums of trefoils) we have seen that at a given length, polygons of knot type $3_1^+\#3_1^-$ are roughly twice as numerous as those of knot type $3_1^+\#3_1^+$. Generally, polygons with knot types which are connected sums of left- and right-handed trefoils appear to be more numerous than polygons of the same length and knot type which are the connected sum of only left- or right-handed polygons. For example, simulations of knot types $3_1^+\#3_1^+\#3_1^-$ and $3_1^+\#3_1^+\#3_1^+$ show that

$$M_{(3_1^+\#3_1^+\#3_1^-),(3_1^+\#3_1^+\#3_1^+)} = 9.0 \pm 1.4. \tag{5.9}$$

This shows that polygons of knot type $3_1^+\#3_1^+\#3_1^-$ are about 9 times more numerous than with knot type $3_1^+\#3_1^+\#3_1^+$ in the asymptotic limit.

Estimating $M_{0_1,(3_1^+\#3_1^+\#3_1^-)}$ produces results which were very sensitive to the maximum length of polygons in our data. Discarding all polygons of length $n > 700$ gave acceptable fits for $n_{min} = 68$. Our best estimate (using $N_K = 3$) was $[C_{0_1}/C_{3_1^+\#3_1^+\#3_1^-}] = 39.595 \pm 0.066$ so that

$$M_{0_1,(3_1^+\#3_1^+\#3_1^-)} = (1.08 \pm 0.11) \times 10^6, \tag{5.10}$$

where we noted that that $3_1^+\#3_1^+\#3_1^-$ is chiral. This is less that the estimate of $M_{0_1,(3_1^+\#3_1^+\#3_1^+)}$ in equation (5.5), implying that this compound knot is more numerous.

To further investigate this we also attempted simulations for the knot types $(3_1^+)^2\#(3_1^-)^2$. This knot type proved beyond the capacity of our available computers – sieving out the shortest knots to set a scale for the simulation produced tens of millions of polygons (far more than the 2752304 found for $(3_1^+)^4$. Our preliminary results are enough however to support the following conjecture about the frequencies of knots types.

Conjecture: Consider the knot types

$$K_+(N) = (3_1^+)^{\lceil N/2 \rceil}\#(3_1^-)^{\lfloor N/2 \rfloor} \quad \text{and}$$
$$K_-(N) \quad = (3_1^-)^{\lceil N/2 \rceil}\#(3_1^+)^{\lfloor N/2 \rfloor}$$

where $K_+(0) = K_-(0) = 0_1$, $K_+(1) = 3_1^+$ and $K_-(1) = 3_1^-$. Then amongst polygons of a given even length $n \geq 4$ there is an N such that the most populous knot types are both $K_+(N)$ and $K_-(N)$. Moreover, N increases to infinity proportionally with n, so that the complexity of the most populous knot type increases with the length of the polygons. ♢

This conjecture in particular is also consistent with $p_n(3_1^+\#3_1^-) > p_n(3_1^+\#3_1^+)$ for each value of n. It is also supported by the estimates in equations (5.7), (5.8), and (5.9).

6. Conclusions

In this paper we have presented approximate enumeration data for polygons of fixed knot types generated by using the GAS algorithm [23,20]. The algorithm was implemented using elementary BFACF moves as atmospheric moves.

As part of the implementation, we sieved knotted polygons of minimal length for many different knot types. Our results confirm numerical data obtained elsewhere [42,43]. In addition, we were able to examine the numbers of symmetry classes of minimal lattice knots. In most of the knot types we have examined, each symmetry class contained 24 distinct polygons under rotations and reflections in the octahedral group. Amongst the prime knot types we examined, only the knot types 0_1, 3_1, 6_1 and 8_{19} produced minimal length conformation which are symmetric with respect to some elements of the octahedral group. In all the other cases, each minimal conformation belonged to a symmetry class of 24 distinct members under action of cubic lattice symmetries. Amongst the compounded knots we considered, the knot types $3_1^+\#3_1^+$, $3_1^+\#3_1^-$, $4_1\#4_1$ and $3_1^+\#3_1^+\#3_1^+\#3_1^+$ had symmetric embeddings. Overall it appears that symmetric embeddings were the exception, rather than the rule, and we expect this pattern to persist.

Careful extrapolation of our numerical estimates of $p_n(K)$ allowed us to both examine (1) the relative frequencies of knot types in asymptotic long polygons, and (2) the values of n (the lengths of polygons) at which various knot types start to dominate in a relative sense. For example, we estimates that $[p_n(3_1^\pm)/p_n(4_1)] \to 27.0\pm2.2$ as $n \to \infty$, and while $p_n(3_1^\pm) \leq p_n(\emptyset)$ for small values of n, one nevertheless expects that $p_n(3_1^\pm) > p_n(\emptyset)$ if $n \geq M_{0_1,3_1}$ where $M_{0_1,3_1} \approx 170000$. Similar results were obtained for other knot types, and in the cases we have examined in this paper, it is possible for us to state with some level of certainty the dominating knot types at a given value of n.

These results produced strong support for a conjecture about the most popular knot-types in cubic self-avoiding polygons. While the probability that a polygon will have a particular knot type goes to zero as its length increases, we conjecture that the probability distribution over knot types peaks on knots of type $K_+(N)$ and $K_-(N)$ for polygons of every fixed length n. Moreover, we predict that N will increase proportionally with n (where N is the number of prime factors of type $3_1^\pm$).

We are continuing our investigations of this conjecture and in particular of our results on the relative frequencies of knot types as defined by $M_{K,L}$. In particular, if K and L are both prime knot types, or have the same number of prime components, then $M_{K,L}$ is dimensionless, and may in fact be universal (independent of the lattice). Currently we are examining this by computing $M_{K,L}$ for other three dimensional lattices.

Acknowledgments: EJJvR and AR are grateful to R. Scharein for making available some of his data, and for commenting on our results. EJJvR and AR acknowledge support in the form of a Discovery Grants from NSERC (Canada).

References

[1] Aragão de Carvalho C, Caracciolo S and Fröhlich J 1983 *Polymers and $g|\phi|^4$-theory in Four Dimensions*, Nucl. Phys. B**215** [FS7] 209-248
[2] Berg B and Foester D 1981 *Random Paths and Random Surfaces on a Digital Computer*, Phys. Lett. **106B** 323-326
[3] Bachmann M and Janke W 2003 *Multicanonical chain-growth algorithm*, Phys. Rev. Lett. **91**, 208105
[4] Clisby N, Liang R and Slade G 2007 *Self-Avoiding Walk Enumeration via the Lace Expansion*. J. Phys. A: Math. Theor. **40** 10973-1017
[5] de Gennes P G 1979 *Scaling Concepts in Polymer Physics*. Cornell University Press (New York)
[6] Diao Y 1993 *Minimal knotted polygons on the cubic lattice*. J. Knot Theor. Ram. **2** 413-425
[7] Diao Y 1994 *The Number of Smallest Knots on the Cubic Lattice*. J Stat Phys **74** 1247-1254
[8] Flory P J 1955 *Statistical Thermodynamics of Semi-Flexible Chain Molecules*. Proc. Roy. Soc. (London) A **234** 60-73
[9] Flory P J 1969 *Statistical Mechanics of Chain Molecules*. Wiley Interscience: New York
[10] Grassberger P 1997 *Pruned-Enriched Rosenbluth Method: Simulation of θ-polymers of Chain Length up to 1 000 000*. Phys. Rev. E **56** (1997), 3682-3693
[11] Guida R and Zinn-Justin J 1998 *Critical Exponents of the N-vector Model*. J. Phys. A: Math. Gen. **31** 8103-8121
[12] Hammersley J M 1960 *Limiting Properties of Numbers of Self-Avoiding Walks*. Phys. Rev. **118** 656-656
[13] Hammersley J M 1961 *The Number of Polygons on a Lattice*. Math. Proc. Camb. Phil. Soc. **57** 516-523
[14] Hammersley J M and Morton K W 1954 *Poor Man's Monte Carlo*. J Roy Stat Soc B **16** 23-38
[15] Janse van Rensburg E J 1995 *Lattice Invariants for Knots*. In *Mathematical Approaches to Biomolecular Structure and Dynamics*. Eds J P Mesirov, K Schulten and D W Sumners. Proc IMA Summer Prog in Mol Biol 11-20 (Springer-Verlag, New York, 1995)
[16] Janse van Rensburg E J 1992 *Ergodicity of the BFACF Algorithm in Three Dimen-*

sions. J Phys A: Math Gen **25** 1031-1042

[17] Janse van Rensburg E J 2002 *The Probability of Knotting in Lattice Polygons.* In *Physical Knots: Knotting, Linking, and Folding Geometric Objects in*R^3. Eds. J. A. Calvo, K. C. Millett, and E. J. Rawdon. *Contemporary Mathematics* **304** (American Mathematical Society, Providence, Rhode Island), 125-135

[18] Janse van Rensburg E J 2007 *Squeezing Knots.* J Stat Mech: Theo Expr **03** P03001

[19] Janse van Rensburg E J 2009 *Monte Carlo Methods for the Self-Avoiding Walk.* J Phys. A: Math. Theo. **42** 323001-97

[20] Janse van Rensburg E J 2009 *Approximate Enumeration of Self-Avoiding Walks.* To appear in *Contemporary Mathematics.*

[21] Janse van Rensburg E J and Promislow S D 1995 *Minimal Knots in the Cubic Lattice.* J. Knot Theo. Ram. **4** 115-130

[22] Janse van Rensburg E J and Rechnitzer A 2008 *Atmospheres of Polygons and Knotted Polygons.* J Phys. A: Math. Theo. **41** 105002-25

[23] Janse van Rensburg E J and Rechnitzer A 2009 *Generalised Atmospheric Sampling of Self-Avoiding Walks.* J Phys. A: Math. Theo. **42** 335001-30

[24] Janse van Rensburg E J and Whittington S G 1991 *The BFACF Algorithm and Knotted Polygons.* J Phys A: Math Gen **24** 5553-5567

[25] Jensen I 2003 *A Parallel Algorithm for the Enumeration of Self-Avoiding Polygons on the Square Lattice.* J Phys. A: Math. Gen. **36** 5731-5745

[26] Jensen I and Guttmann A J 1999 *Self-Avoiding Polygons on the Square Lattice.* J. Phys. A: Math. Gen. **32** 4867-4876

[27] Kesten H 1963 *On the Number of Self-Avoiding Walks.* J. Math. Phys. **4** 960-969

[28] Kesten H 1964 *On the Number of Self-Avoiding Walks II.* J. Math. Phys. **5** 1128-1137

[29] Le Guillou J C and Zinn-Justin J 1989 *Accurate Critical Exponents from Field Theory.* J. de Physique **50** 1365-1370

[30] Madras N and Slade G 1993 *The Self-Avoiding Walk.* (Birhäuser: Boston)

[31] Madras N and Sokal A D 1987 *Nonergodicity of Local, Length-preserving Monte Carlo Algorithms for the Self-Avoiding Walk.* J Stat Phys **47** 573-595

[32] Marcone, Orlandini, Stella, Zonta 2007 *Size of Knots in Ring Polymers.* Phys. Rev. E **75** 041105

[33] Nienhuis B 1982 *Exact Critical Point and Critical Exponents on* $O(n)$ *Models in Two Dimensions. Phys. Rev. Lett.* **49** 1062-1065

[34] Nienhuis B 1984 *Coulomb Gas Formulation of the Two-Dimensional Phase Transitions.* In *Phase Transitions and Critical Phenomena* **11** 1-53. Eds. C. Domb and J.L. Lebowitz (Academic Press)

[35] Orlandini E, Tesi M C, Janse van Rensburg E J and Whittington S G 1998 *Asymptotics of Knotted Lattice Polygons.* J. Phys. A: Math. Gen. **31** 5953-5967

[36] Pippenger N 1989 *Knots in Self-Avoiding Walks.* Disc. Appl. Math. **25** 273-278

[37] Prellberg T and Krawczyk J 2004 *Flat Histogram Version of the Pruned and Enriched Rosenbluth Method.* Phys Rev Lett **92** 120602-5

[38] Eric J. Rawdon, Akos Dobay, John C. Kern, Kenneth C. Millett, Michael Piatek, Patrick Plunkett, and Andrzej Stasiak 2008 *Scaling Behavior and Equilibrium Lengths of Knotted Polymers.* Macromolecules, **41**(12) 4444-4451

[39] Rechnitzer A and Janse van Rensburg E J 2002 *Canonical Monte Carlo Determination of the Connective Constant of Self-Avoiding Walks.* J. Phys. A: Math. Gen. **35** L605-L612

[40] A. Rechnitzer and E.J. Janse van Rensburg *Generalised Atmospheric Rosenbluth Methods (GARM).* J. Phys. A: Math. Theo. **41** (2008), 442002-10

[41] M.N. Rosenbluth and A.W. Rosenbluth *Monte Carlo Calculation of the Average*

Extension of Molecular Chains. J. Chem. Phys. **23** (1955), 356-359

[42] Scharein R, Ishihara K, Arsuaga J, Diao Y, Shimokawa K and Vazquez M 2009 *Bounds for minimal step number of knots in the simple cubic lattice*. J. Phys. A: Math. Theor. 42 (2009) 475006-30

[43] Scharein R 2010 Private communication

[44] Sumners D W and Whittington S G 1988 *Knots in Self-Avoiding Walks*. J. Phys. A: Math. Gen. **21** 1689-1694